Title

Determinations of Uranium Structures by EXAFS: Schoepite and Other U(VI) Oxide Precipitates

Author

Allen, Patrick G.

Publication Date

1995-12-16

LBL-38198
UC-401
Preprint

Lawrence Berkeley Laboratory
UNIVERSITY OF CALIFORNIA

CHEMICAL SCIENCES DIVISION

Submitted to Radiochimica Acta

Determinations of Uranium Structures by EXAFS: Schoepite and Other U(VI) Oxide Precipitates

P.G. Allen, D.K. Shuh, J.J. Bucher, N.M. Edelstein, C.E.A. Palmer, R.J. Silva, S.N. Nguyen, L.N. Marquez, and E.A. Hudson

December 1995

Prepared for the U.S. Department of Energy under Contract Number DE-AC03-76SF00098

DISCLAIMER

LBL-38198
UC-401

Determinations of Uranium Structures by EXAFS: Schoepite and Other U(VI) Oxide Precipitates

P.G. Allen,[1,2] D.K. Shuh,[1] J.J. Bucher,[1] N.M. Edelstein,[1] C.E.A. Palmer,[2]
R.J. Silva,[2] S.N. Nguyen,[2] L.N. Marquez,[2] and E.A. Hudson[2]

[1]Chemical Sciences Division
Lawrence Berkeley National Laboratory
University of California
Berkeley, California 94720

[2]G.T. Seaborg Institute for Transactinium Science
Lawrence Livermore National Laboratory
Livermore, California 94551

December 1995

This work was supported by the Director, Office of Energy Research, Office of Basic Energy Sciences, Chemical Sciences Division, of the U.S. Department of Energy under Contract No. DE-AC03-76SF00098.

Determinations of Uranium Structures by EXAFS: Schoepite and Other U(VI) Oxide Precipitates

P. G. Allen,[1,2*] D. K. Shuh,[1] J. J. Bucher,[1] N. M. Edelstein,[1]

C. E. A. Palmer,[2] R. J. Silva,[2] S. N. Nguyen,[2] L. N. Marquez,[2] and E. A. Hudson[2]

[1]Chemical Sciences Division, Lawrence Berkeley National Laboratory, Berkeley, CA 94720

[2]G.T. Seaborg Institute for Transactinium Science,

Lawrence Livermore National Laboratory, Livermore, CA 94551

Abstract

We have investigated the structures of U(VI) oxides precipitated from room temperature aqueous solutions at low ionic strength as a function of pH. Using the uranium L_{III} - edge extended x-ray absorption fine structure (EXAFS) and infrared (IR) spectroscopies as probes of the local structure around the uranium, a trend is observed whereby the axial oxygen bond lengths from the uranyl groups increase from 1.80 Å at pH=7 to 1.86 Å at pH=11. Shifts in the IR spectral frequencies support this assignment. A concomitant decrease in the equatorial oxygen and nearest-neighbor uranium bond lengths also occurs with increasing pH. Expansion of the linear O=U=O group is seen directly at the L_{III} absorption edge where multiple scattering resonances systematically shift in energy. EXAFS curve-fitting analysis on these precipitates and a sample of synthetic schoepite indicate that the structure of the species formed at pH=7 is similar to the structure of schoepite. At pH=11, the precipitate structure is similar to that of a uranate.

Introduction

Understanding the migration properties of radionuclides in the environment is vital for developing safe and effective long-term methods for the storage of nuclear materials. To accurately model radionuclide migration, it is important to identify the source terms and determine their speciation (i.e., thermodynamics, red-ox properties, molecular structure). This task becomes more difficult when the primary source term has the propensity to transform into a secondary phase which effectively becomes the solubility-controlling solid. Spent nuclear reactor fuel is one such example where in an oxidizing environment, UO_2 transforms [1-4] into UO_2^{2+}-containing solid phases, i.e., $UO_2(OH)_2 \cdot H_2O$ (schoepite). For the uranyl ion, UO_2^{2+}, the solubility equilibria and the corresponding controlling solids depend on the ionic strength and the type of medium, temperature, and pH. In this report, we describe a systematic study of the structures of uranium (VI) oxides that are formed in dilute sodium sulfate solutions as a function of pH.

Numerous structural determinations have been made on uranium(VI) oxides [5-10], hydroxides [11,12] and alkali metal uranates [10, 13-15]. In contrast, the structure of the hydrated oxide, $UO_2(OH)_2 \cdot H_2O$, has been studied by x-ray diffraction (XRD), but atomic coordinates have yet to be determined [16-21]. The difficulty in obtaining a detailed structure by XRD for natural as well as synthetic schoepite polymorphs most likely arises from the tendency towards amorphous structures in these materials, owing to the variability in the degree of hydration. With the advent of x-ray absorption fine structure (EXAFS) spectroscopy, it is possible to determine local structure around almost any atom even when long-range order does not exist. As a result, we have sought to determine the structure of synthetic schoepite along with solids that are precipitated from dilute sulfate solutions as a function of pH using EXAFS.

Experimental

1. Sample Preparation

All solutions were prepared using CO_2-free, double-distilled and deionized water from a Millipore Corp. purification system. The chemicals used were $UO_2(NO_3)_2 \cdot 6H_2O$ (s), HCl, NaOH(s), NaCl(s) (Merck, analytical grade), and Na_2SO_4(s) (EM science, ultrapure grade). The pH measurements were made with an Orion Model 611 pH meter and an Orion 8103 BN electrode. Stock solutions of ^{238}U were made by dissolving an appropriate amount of uranyl nitrate in concentrated HCl (12 M) and were purified from daughter activities using an anion exchange column. The titrations and subsequent precipitation reactions were carried out in an argon (Ar)-filled, CO_2-free glove box. Schoepite was precipitated from a supersaturated solution of 0.1 mM uranyl ion in 0.1 M hydrochloric acid by addition of 1.0 M NaOH and was kept at pH=7 [22]. The XRD pattern obtained for the precipitated yellow solid matched that of metaschoepite which has been reported in the literature [18, 23].

A second series of precipitation reactions was carried out as a function of pH using a uranium stock solution consisting of 0.1 M uranyl ion in 1.0 M hydrochloric acid. 0.6 ml aliquots of this solution were added to three 100 ml portions of a 1.0 mM Na_2SO_4 solution. The pH of each mixture was adjusted with 1.0 M NaOH to the values of 7.2, 9.1, and 10.6. The final concentrations of each ionic species in solution were: $[UO_2^{2+}]$=0.6 mM, $[Cl^-]$=6 mM, $[SO_4^{2-}]$=1 mM, and $[Na^+]$=50 mM. The solutions were gently stirred with an Orbit shaker for 9 weeks. At the end of this period, the experiment was stopped and the pH values were remeasured at 7.2, 8.2, and 11.4. The precipitated solids (~10 mg each) were recovered by pressure membrane filtration and allowed to dry under atmosphere. The colors of the solids ranged from yellow at pH=7 to orange at pH=11.

2. EXAFS and FTIR Data Acquisition.

Approximately 5 mg of the precipitates (labeled as pH-7, pH-9, and pH-11) were mixed with boron nitride (BN) powder and placed in 1.5 x 20 mm slots cut out from 1.5 mm thick polyethylene frames. The samples were sealed in the slots with Kapton tape which served as x-ray

transparent windows. The schoepite sample was prepared in an analogous manner using an aluminum holder (for low-temperature measurement). The resulting U cross-section in these mixtures yielded an edge jump ~1.0 across the uranium L_{III} absorption edge. Uranium L_{III}-edge x-ray absorption spectra were collected at the Stanford Synchrotron Radiation Laboratory (SSRL) on wiggler beamline 4-3 (unfocused) under dedicated ring conditions (3.0 GeV, 50-100 mA) using a Si (220) double-crystal monochromator. All spectra were collected in the transmission geometry using argon-filled ionization chambers and a vertical slit of 0.5 mm. The pH-7, pH-9, and pH-11 samples were measured at room temperature, and schoepite was measured at 20 K using an Oxford Instruments continuous-flow liquid helium cryostat. Rejection of higher order harmonic content of the beam was achieved by detuning θ, the angle between crystals in the monochromator, such that the incident flux was reduced to 50% of its maximum (>95% harmonic is rejected). Three EXAFS scans were collected from each sample, and the results were averaged. The spectra were energy calibrated by simultaneously measuring the spectrum from a reference solution of 0.2 M UO_2Cl_2 which was placed between the second and third ionization chambers. The first inflection point of the absorption edge for the reference was defined as 17166 eV. The EXAFS data were extracted from the raw absorption spectra by standard methods described elsewhere [24] using the suite of programs EXAFSPAK developed by G. George of SSRL. Non-linear least squares curve-fitting analysis was done using EXAFSPAK to fit the raw k^3-weighted EXAFS data.

The theoretical EXAFS modeling code, FEFF6, of Rehr *et al.* [25] was employed to calculate the backscattering phases and amplitudes of the individual neighboring atoms for the purpose of curve-fitting the raw data. All of the interactions modeled in the fits were derived from FEFF6 single or multiple scattering paths (SS or MS) calculated for the model compound, α-$UO_2(OH)_2$ [11]. The relevant paths that FEFF6 calculates for this model compound are SS U–O (axial), SS U–O (equatorial), MS O–U–O (4 legged path), and SS U–U. The MS interaction occurs at ~3.6 Å and is derived from a path along the O–U–O vector which is twice the U–O_{ax} distance. This was included in the fits as a parameter linked directly to floating bond lengths (R) and coordination number (*N*) values of the axial oxygen shell [26]. The amplitude reduction

factor, S_0^2, was held fixed at 0.9 for all of the fits. The shift in threshold energy, ΔE_0, was allowed to vary as a global parameter for the O and U atoms in each of the fits (i.e., a single value of ΔE_0 was used for all the O shells and another ΔE_0 was used for the U shells).

Fourier-transform infrared (FTIR) absorption spectroscopy was performed with a Mattson Galaxy FTIR Series 5000 system over the range of 3000 to 300 cm^{-1}. 5 mg of each sample was finely ground, mixed with KBr, and pressed into 13 mm diameter disks. A pure disk of KBr was used as a reference sample.

Results

1. EXAFS

Figure 1 shows the raw k^3-weighted EXAFS data for pH-11, pH-9, pH-7, and schoepite. Upon initial inspection, all of the spectra are quite similar and show good signal-to-noise which extends the useful range of the data out to k~15 $Å^{-1}$. The low-k region is dominated by a low frequency oscillation which arises from back-scattering of the oxygen atoms in the uranyl group, while at high-k, the spectra show a high frequency pattern emerging which at this level can be attributed to the presence of more distant atoms having a large cross-section, (i.e. uranium). However, closer inspection of the k-space plots reveals several differences among the data. Specifically, the pH-11 and pH-9 samples show a strong resemblance in their high k fine structure which is different than the fine structure observed for the pH-7 and schoepite solids. The difference is particularly apparent at k=15 $Å^{-1}$ where the oscillations in the pH-11 and pH-9 samples are π (180 degrees) out of phase with the oscillations in the pH-7 and schoepite samples. In contrast, the oscillations at high-k for schoepite are in phase with pH-7, although they are more pronounced and better resolved in schoepite as a result of thermal damping (schoepite was measured at 20 K).

The trends noted in the k-space data are more apparent in the R-space plots of the Fourier transformed EXAFS spectra shown in Figure 2. The Fourier transforms (FTs) represent a pseudo-radial distribution function of the uranium near-neighbor environment, and the peaks

appear at lower R values relative to the true near neighbor distances as a result of the electron scattering phase shifts which are different for each neighboring atom (α=0.2-0.5 Å). The FTs illustrate that the EXAFS spectra are dominated by backscattering from the O atoms of the linear UO_2^{2+} group (peak at 1.30 Å) [26-30]. Backscattering from the O atoms lying in the equatorial plane of the UO_2^{2+} ion is observed in the pH-7 and schoepite data sets as shown by the pattern of FT peaks centered around 1.90 Å. Moving from pH-7 to pH-11, a structural transformation is observed in the precipitates as the 1.30 Å peak broadens, shifts to higher R, and the pattern in the equatorial O region is lost. In addition, all of the spectra exhibit a feature(s) at ~ 3.6 Å, which is attributed to backscattering from more distant U neighbors. Low Z atoms are not normally detected at R > 3 Å, unless a multiple scattering enhancement of the amplitude is present. Examples of this have been observed when ligands like carbonate or nitrate adopt a symmetric bidentate geometry with the distal O atom being collinear with the absorbing atom and the C or N atoms [26,31]. However, this type of configuration is not possible in our samples since nitrate and carbonate were not present in the preparations. Accompanying the changes observed for the oxygen atoms, the positions of the U peaks shift to lower R upon going from pH-7 to pH-11.

Non-linear least squares curve-fitting was done over the range 3–15 $Å^{-1}$ on the raw EXAFS data to examine the nature of the structural transformations more quantitatively. The corresponding fits are shown in Figures 1 and 2, and the bond lengths and coordination numbers are summarized in Table 1. Although these samples may contain a mixture of phases (EXAFS detects average structure), the structural differences and similarities are easily discerned. The sample pH-7 closely resembles schoepite with ~2 O at 1.80 Å, a split shell of ~4 equatorial O atoms at 2.26 Å and 2.48 Å, and ~1 U at 3.87 Å. Schoepite also shows ~1 U at 4.53 Å, the detection of which is likely due to a more homogeneous sample as well as the low temperature measurement (which reduces thermal damping). As the pH of the precipitation reactions increases from 7 to 9 and 11, the axial oxygen bond lengths increase to 1.84 Å and 1.86 Å, respectively while the equatorial bond lengths remain split and, on average, show a decrease. The inverse relation between axial and equatorial O bond lengths has been observed for a variety of uranium

(VI) compounds previously [32]. The shell of U atoms becomes split at pH-9 and -11, with ~ 1 U at 3.71 Å and ~1 U at 3.92 Å (pH-9) and 4.21 Å (pH-11). All of the structural trends observed in the FTs are confirmed by the curve-fitting results.

2. X-ray Absorption Near-Edge Structure (XANES)

The normalized U L_{III}-edges for pH-7, pH-9, and pH-11 are shown in Figure 3a. The primary absorption peak at 17.17 keV is associated with an allowed $2p \rightarrow 6d$ transition. The shoulder that appears at *ca.* 17.18 keV has been observed in the L_{III} XANES of numerous U(VI) oxides [33-36], where it has been proposed to originate from MS resonances that are associated with the relatively short U-O bond interaction of the uranyl group. This assignment has been confirmed more recently by detailed XANES calculations using FEFF6 [37]. As the pH increases, the position of the MS resonance systematically shifts to lower energy. This behavior follows the inverse relation observed in earlier studies between the positions of MS resonances and bond lengths [38,39].

The U L_{III} XANES for pH-7, pH-9, and pH-11 were modeled using FEFF6 and the structure from the model compound α-$UO_2(OH)_2$ [11]. The calculations were done using a 5 Å radius cluster with the uranium atom at the center. Different atomic potentials were used for the axial and equatorial oxygen atoms due to their substantially different environments. The U and O potentials were then automatically overlapped, and a 3 eV correction was applied to the relative position of the Fermi level. In order to simulate the shifts in the position of the MS resonance, the $U–O_{axial}$ bond lengths were varied using the values obtained from the EXAFS curve-fits, 1.80 Å, 1.84 Å, and 1.86 Å. The results of the simulations are shown in Figure 3b. As can be seen, the calculations are quite accurate at simulating both the MS resonance shape and its energy shift as a function of pH. In addition, the calculations also adequately model the shift in the peak at 17.21 keV. Similar results are obtained when the changes in the positions of the equatorial atoms are included, verifying that scattering from the axial oxygen atoms is the primary origin of the observed effects. Thus, the U XANES also serves as a probe for following structural change in these precipitates.

3. Infrared Spectroscopy

The infrared absorption spectra of schoepite, pH-7, pH-9, and pH-11 are shown from 1400 to 300 cm^{-1} in Figure 4. All of the spectra exhibited higher energy bands (not shown) assigned to water in each sample. The spectrum of schoepite is nearly identical to that reported by Hoekstra and Siegel [19], apart from slight differences in the resolution of the respective bands. The prominent uranyl absorption band peaks from the schoepite sample are at 885 and 930 cm^{-1}. These have previously been assigned to the symmetric stretching (ν_1) and asymmetric stretching (ν_3) vibrations, where the appearance of a symmetric vibration in the IR occurs due to symmetry breaking by the crystal field [5]. However, the possibility of multiple phases in the pH-7, pH-9, and pH-11 samples makes the assignment of the peaks in the spectra more difficult. As a result, it is more instructive to look at the general trends displayed in the spectra. As the pH increases, there is a gradual transformation in the 930-850 cm^{-1} region to the lower frequency vibration. In the pH-7 sample, the principal peak is at 910 cm^{-1}, while for the pH-11 sample, the main peak appears at 865 cm^{-1}. The absence of U–O vibrations above 900 cm^{-1} is likely to result [5, 40] from bridging of the uranyl axial oxygens to other atoms in the structure (uranyl groups are no longer "free") and may also reflect an overall lengthening of the $U–O_{axial}$ bonds. The peak assigned to the deformation mode, δ(U–O–H), [19] follows the trend 999, 1003, and 1007 cm^{-1} with increasing pH which is consistent with tightening (shortening) of the equatorial O bonds.

Discussion

The $U–O_{axial}$ bond lengths are 1.80, 1.84, and 1.86 Å in pH-7,-9, and -11 oxide samples, and the average $U–O_{equatorial}$ bond lengths are 2.38, 2.36, 2.32 Å, respectively. These trends along with the contraction of the U–U bonds with increasing pH suggest the structural changes shown in Figure 5. In pH-7 the precipitated solid resembles schoepite, or a similar hydrated uranyl hydroxide. In pH-11, the uranyl group becomes elongated and the equatorial bonds contract as the structure more closely resembles that of an alkali metal uranate. The pH-9 sample has a structure which is intermediate between the others. The EXAFS curve-fitting results as well

as the IR data support these assignments. The pH-7 precipitate possesses U–O bond lengths indicative of the schoepite sample reported here, while the pH-11 sample has U–O bond lengths which are closer to those found in the structural determinations of Na_2UO_4,[41] $Na_2U_2O_7$, [42] and $K_2U_7O_{22}$ [43].

The correspondence between the structures of pH-7 and schoepite may be explained by the nearly identical chemical conditions for each (i.e., low ionic strength and pH=7). Apparently the presence of dilute sulfate has little effect on the structure of the precipitated solid. Although the synthesis of sodium uranates typically has been done at high temperature and in the solid state [41-46], it is possible to form the same structures from precipitation reactions using uranyl nitrate solutions at high pH [47-49]. Analogous to the pH-11 solid that was formed in the presence of dilute sulfate, precipitated polyuranates [48] and many of the monouranates [10] are orange in color. However, Na_2UO_4 is hygroscopic [45], and chemically, the formation of a polyuranate rather than a monouranate is favored in room temperature solutions at pH=11 [48]. In fact, the IR spectra of pH-11 resembles that of $Na_2U_2O_7$ more closely than any of the monouranates [44-46]. Furthermore, the pH-11 sample must be a hydrated form of a polyuranates since there are water bands and δ(U–O–H) modes in the IR. Thus, it is likely that the pH-11 sample is a hydrated uranate possibly analogous to ones reported previously (i.e., $Na_2U_3O_{10}\cdot xH_2O$), although detailed structures with atomic positions have not been reported for these compounds [50].

Finally, disorder seems to be the rule in these structures. The U–O bond lengths for the mono- and diuranates along with those of $UO_2(OH)_2$ phases show that there is an extreme amount of static disorder, particularly in the equatorial plane. The presence of disorder, and the tendency towards amorphous structures is further demonstrated by the lack of reported atomic positions for these compounds (i.e., polyuranates and schoepite). The observation of a split equatorial shell is an indication of disorder in the precipitates described herein. It is possible that the equatorial shells in these samples possess more than just two discrete distances. However these were either unresolvable given the resolution of the EXAFS data, ΔR=0.10 Å [51], or did not offer a statistically significant improvement in the fit. Despite this limitation, the EXAFS results are able

to discern the structural trends in these samples. In this regard, EXAFS spectroscopy is particularly useful for extracting structural information from materials that do not exhibit long-range ordered diffraction behavior and should find increasing application to such systems.

Acknowledgments

This work was supported by the Director, Office of Energy Research, Office of Basic Energy Sciences, Chemical Sciences Division of the U. S. Department of Energy under Contract No. DE-AC03-76SF00098. This work was done at SSRL which is operated by the Department of Energy, Division of Chemical Sciences.

References

1. Finch, R. J., Miller, M. L., Ewing, R. C.: Weathering of Natural Uranyl Oxide Hydrates: Schoepite Polytypes and Dehydration Effects. Radiochim. Acta **58/59**, 433-443 (1992).
2. Sandino, M. C. A., Grambow, B.: Solubility Equilibria in the U(VI)-Ca-K-Cl-H_2O System: Transformability of Schoepite into Becquerelite and Compreignacite. Radiochim. Acta **66/67**, 37-43 (1994).
3. Torrero, M. E., Casa, I., de Pablo, J., Sandino, M. C. A., Grambow, B.: A Comparison Between Unirradiated UO_2(s) and Schoepite Solubilities in 1 M NaCl Medium. Radiochim. Acta **66/67**, 29-35 (1994).
4. Kim, W. H., Choi, K. C., Park, K. K., Eom, T. Y.: Effects of Hypochlorite Ion on the Solubility of Amorphous Schoepite at 25°C in Neutral to Alkaline Aqueous Solutions. Radiochim. Acta **66/67**, 45-49 (1994).
5. Hoekstra, H. R., Siegel, S.: The Uranium-Oxygen System: U_3O_8–UO_3. J. Inorg. Nucl. Chem. **18**, 154-165, (1961).
6. Greaves, C., Fender, B. E. F.: The Structure of α-UO_3 by Neutron and Electron Diffraction. Acta Cryst. **B28**, 3609 (1972).
7. Debets, P. C.: The Structure of β-UO_3. Acta Cryst. **21**, 589 (1966).
8. Engmann, R., De Wolff, P. M.: The Crystal Structure of γ-UO_3. Acta Cryst. **16**, 993 (1963).
9. Wait, E.: A Cubic Form of Uranium Trioxide. J. Inorg. Nucl. Chem. **1**, 309-312 (1955).
10. Weigel, F.: Uranium, *The Chemistry of the Actinide Elements*; Eds. J. J. Katz, G. T. Seaborg, and L. R. Morss. Chapman and Hall: New York, Vol. 1, Chapter 5, (1986).
11. Taylor, J. C., Hurst, H. J.: The Hydrogen Atom Locations in the α and β Forms of Uranyl Hydroxide. Acta Cryst. **B27**, 2018-2022 (1971).
12. Siegel, S., Hoekstra, H. R.; Gebert, E.: The Structure of γ-Uranyl Dihydroxide, $UO_2(OH)_2$. Acta Cryst. **B28**, 3469 (1972).

13. Keller, C.: Lanthanide and Actinide Mixed Oxide Systems with Alkali and Alkaline Earth Metals, *MTP International Review of Science, Inorganic Chemistry, Series. 1,* Ed. K. W. Bagnall. Butterworths: London, Vol. 7, Chapter 2 (1972).

14. Morss, L. R.: Complex Oxide Systems of the Actinides, *Actinides In Perspective*, Ed. N. M. Edelstein. Pergamon Press Inc.: New York, 381-408 (1982).

15. Gmelin Handbuch der Anorganischen Chemie, Suppl. Ser. Uranium, Springer-Verlag, Berlin, Heidelberg, and New York. C3 Ternary and Polynary Oxides (1973).

16. Christ, C. L., Clark, J. R.: Crystal Chemical Studies of Some Uranyl Oxide Hydrates. Am. Mineral. **45**, 1026-1061 (1960).

17. Wheeler, V. J., Dell, R. M., Wait, E.: Uranium Trioxide and the UO_3 Hydrates. J. Inorg. Nucl. Chem. **26**, 1829-1845, (1964).

18. Debets, P. C., Loopstra, B. O.: On the Uranates of Ammonium-II: X-ray Investigation of the Compounds in the System NH_3-UO_3-H_2O. J. Inorg. Nucl. Chem. **25**, 945-953, (1963).

19. Hoekstra, H. R., Siegel, S.: The Uranium Trioxide-Water System. J. Inorg. Nucl. Chem. **35**, 761-779, (1973).

20. Peters, J.: Synthèses et étude radiocrystallographique d'uranates synthétiques du type oxyde double d'uranyle. Mem. Soc. Roy. Sci. Liege **14** Fasc. 3, 5-57 (1967).

21. See reference 1 for a detailed review of schoepite and its polymorphs.

22. Silva, R. J., Yee, A. W.: Uranium (VI) Retardation Mechanisms. Lawrence Berkeley Laboratory Earth Sciences Division Annual Report. LBL-13600, 45-47 (1981).

23. JCPDS-ICDD, Powder Diffraction File. Alphabetical index. Inorganic Phases. Diffraction card no. 43-364 (formerly no.18-1436) (1993).

24. *X-ray Absorption: Principles, Applications, Techniques for EXAFS, SEXAFS, and XANES*, Eds. Prins, R., Koningsberger, D. E. Wiley-Interscience: New York, (1988).

25. Rehr, J. J., Mustre de Leon, J., Zabinsky, S., Albers, R. C.: Ab-initio Curved Wave X-ray Absorption Fine Structure. Phys. Rev. B **44**, 4146 (1991).

26. Allen, P. G., Bucher, J. J., Clark, D. L., Edelstein, N. M., Ekberg, S. A., Gohdes, J. W., Hudson, E. A., Kaltsoyannis, N., Lukens, W. W., Neu, M. P., Palmer, P. D., Reich. T., Shuh, D. K., Tait, C. D., Zwick, B. D.: Multinuclear NMR, Raman, EXAFS, and X-ray Diffraction Studies of Uranyl Carbonate Complexes in Near-neutral Aqueous Solution. Inorg. Chem. **34**, 4797 (1995).

27. Chisholm-Brause, C., Conradson, S.D., Buscher, C.T., Eller, P.G., and Morris, D.E.: Speciation of Uranyl Sorbed at Multiple Binding Sites on Montmorillonite. Geochim. Cosmochim. Acta **58**, 3625-3631 (1994).

28. Dent, A.J., Ramsay, J. D. F., Swanton, S. W.: An EXAFS Study of Uranyl Ion in Solution and Sorbed onto Silica and Montmorillonite Clay Colloids. J. Colloid and Interface Sci. 150, **45** (1992).

29. Charpin, P., Dejean, A., Folcher, G., Rigny, P., Navaza, P.: EXAFS sur des Composes de Coordination de L'Uranium en Phase Solide et en Solution. J. Chim. Physique **82**, 925-932 (1985).

30. Waite, T. D., Davis, J. A., Payne, T. E., Waychunas, G. A., Xu, N.: Uranium (VI) Adsorption to Ferrihydrite: Application of a Surface Complexation Model. Geochim. Cosmochim. Acta **58**, 5465 (1994).

31. Veirs, D. K., Smith, C. A., Berg, J. M., Zwick, B. D., Marsh, S. F., Allen, P. G., Conradson, S. D.: Characterization of the Nitrate Complexes of Pu(IV) using Absorption Spectroscopy, ^{15}N NMR, and EXAFS. J. Alloys and Compounds **213/214**, 328 (1994).

32. Veal, B. W., Lam, D. J., Carnall, W. T., Hoekstra, H. R.: X-ray Photoemission Spectroscopy of Hexavalent Uranium Compounds. Phys. Rev. B **12**, 5651 (1975).

33. Farges, F., Ponader, C.W., Calas, G., Brown, G.E., Jr.: Structural Environments of Incompatible Elements in Silicate Glass/Melt Systems: II. U(IV), U(V), and U(VI). Geochim. Cosmochim. Acta **56**, 4205 (1992).

34. Petiau, J., Calas, G., Petitmaire, D., Bianconi, A., Benfatto, M., Marcelli, A.: Delocalized versus Localized Unoccupied 5f States and the Uranium Site Structure in Uranium Oxides and Glasses Probed by X-ray Absorption Near-Edge Structure. Phys. Rev. B **34**, 7350 (1986).

35. Kalkowski, G., Kaindl, G., Brewer, W.D., Krone, W.: Near-edge X-ray Absorption Fine Structure in Uranium Compounds. Phys. Rev. **B 35**, 2667 (1987).

36. Bertram, S., Kaindl, G., Jove, J., Pages, M., Gal, J.: Electronic Structure of Actinide Compounds from L_{III}-Edge X-ray Absorption. Phys. Rev. Lett. **63**, 2680 (1989).

37. Hudson, E. A., Rehr, J. J., Bucher, J. J.: Multiple-Scattering Calculations of the Uranium L_{III} X-ray Absorption Near-Edge Structure. Phys. Rev. **B 52**, 13815 (1995).

38. Natoli, C. R.: Distance Dependence of Continuum and Bound State Excitonic Resonances in X-ray Absorption Near-Edge Structure (XANES). *EXAFS and Near-Edge Structure III.* Eds. K. O. Hodgson et al. Springer-Verlag, New York, pp. 38-42 (1984).

39. Bianconi, A., Fritsch, E., Petiau, J.: X-ray Absorption Near-Edge Structure of 3d Transition Elements in Tetrahedral Coordination: The Effect of Bond Length Variation. Phys. Rev. **B 32**, 4292 (1985).

40. Allen, G. C., Holmes, N. R.: Characterization of Binary Oxides by Infrared Spectroscopy. Appl. Spectrosc. **48**, 525 (1994).

41. Kovba, L. M.: Crystal Structures of Potassium and Sodium Monouranates. Soviet Radiochem. **13**, 319-320 (1971).

42. Kovba, L. M.: The Crystal Structure of Sodium Diuranate. Soviet Radiochem. **14**, 727-730 (1972).

43. Kovba, L. M.: Crystal Structure of $K_2U_7O_{22}$. Zhurnal Strukturnoi Khimii. **13**, 256-259 (1972).

44. Cordfunke, E. H. P., Loopstra, B. O.: Sodium Uranates: Preparation and Thermochemical Properties. J. Inorg. Nucl. Chem. **33**, 2427-2436 (1971).

45. Hoekstra, H. R.: Infrared Spectra of Some Alkali Metal Uranates. J. Inorg. Nucl. Chem. **27**, 801-808, (1965).

46. Carnall, W. T., Walker, A., Neufeldt, S. J.: Anhydrous Sodium Polyuranates. Inorg. Chem. **5**, 2135-2140 (1966).

47. Maly, J., Vesely, V.: A Contribution to Sodium Polyuranate Chemistry. J. Inorg. Nucl. Chem. **7**, 119-128, (1958).

48. Wamser, C. A., Belle, J., Bernsohn, E., Williamson, B.: The Constitution of the Uranates of Sodium. J. Am. Chem. Soc. **74**, 1020-1022 (1952).

49. Ricci, J. E., Loprest, F. J.: Phase Relations in the System Sodium Oxide-Uranium Trioxide-Water at 50 and 75°. J. Am. Chem. Soc. **77**, 2119-2129 (1955).

50. JCPDS-ICDD, Powder Diffraction File. Alphabetical index. Inorganic Phases. Diffraction cards no. 41-840 and 12-112 (1993).

51. For shells of identical backscatterers occuring at two different distances R_1 and R_2,the theoretical resolution is given by $\Delta R=\pi/2(k_{max})$.

Figure Captions

Figure 1 Raw U L_{III}-edge k^3-weighted EXAFS data for (A) pH-11, (B) pH-9, (C) pH-7, and (D) schoepite samples. The solid line is the experimental data, and the dashed line represents the best theoretical fit of the data as described in the text.

Figure 2 Fourier transforms of U L_{III} EXAFS for for (A) pH-11, (B) pH-9, (C) pH-7, and (D) schoepite samples. Transforms were taken over the range of the data shown in Figure 1. The solid line is the experimental data, and the dashed line corresponds to the best theoretical fit of the data.

Figure 3. Normalized U L_{III}-edges measured from experiment (A) and calculated from theoretical models (B) for oxide precipitates pH-7, pH-9, and pH-11. The energy shifts of the near-edge resonances are characteristic of changes in the UO_{ax} bond lengths as described in the text.

Figure 4. FTIR absorption spectra for (A) pH-11, (B) pH-9, (C) pH-7, and (D) schoepite samples.

Figure 5. Proposed structural model for the samples pH-7 and schoepite (A); At higher pH (sample pH-11) the precipitate shows an elongation of the axial oxygen bonds and a contraction of the oxygen bonds along the equator (B).

Table 1 EXAFS Structural Results for U(VI) Oxide Precipitates

Schoepite	R(Å)	N	σ^2 (Å^2)[a]	ΔE_0 (eV)
U-O_{ax}	1.80	1.7	0.0014	-10.6
U-O_{eq1}	2.26	2.1	0.0077	-10.6
U-O_{eq2}	2.47	1.9	0.0059	-10.6
U-U	3.84	1.2	0.0023	-17.3
U-U	4.53	1.4	0.0065	-17.3
pH-7				
U-O_{ax}	1.80	1.8	0.0019	-12.6
U-O_{eq1}	2.27	2.7	0.0074	-12.6
U-O_{eq2}	2.49	1.5	0.0059	-12.6
U-U	3.87	1.4	0.0052	-12.2
pH-9				
U-O_{ax}	1.84	2.2	0.0049	-9.4
U-O_{eq1}	2.25	3.5	0.0104	-9.4
U-O_{eq2}	2.47	1.7	0.0131	-9.4
U-U	3.71	1.6	0.0070	-15.7
U-U	3.92	1.4	0.0051	-15.7
pH-11				
U-O_{ax}	1.86	2.1	0.0035	-8.8
U-O_{eq1}	2.24	2.4	0.0057	-8.8
U-O_{eq2}	2.40	1.9	0.0110	-8.8
U-U	3.71	1.2	0.0047	-15.5
U-U	4.21	1.0	0.0068	-15.5

a. σ=Debye-Waller factor

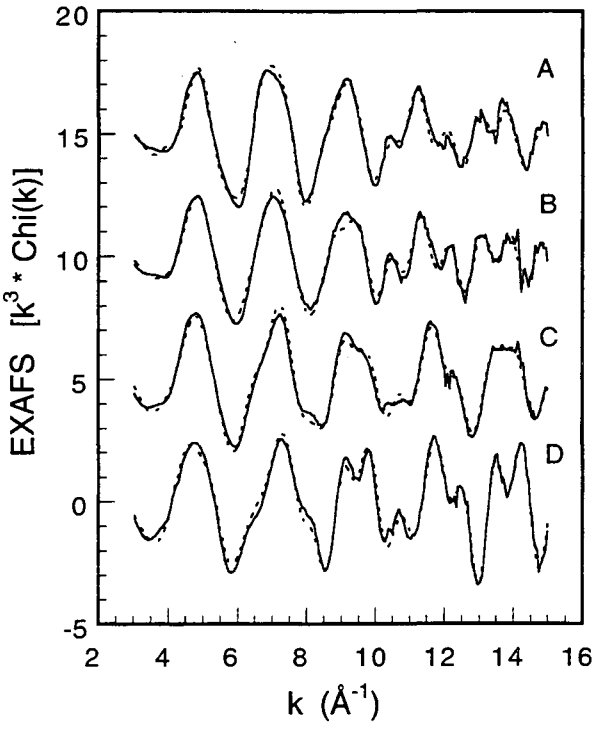

Figure 1

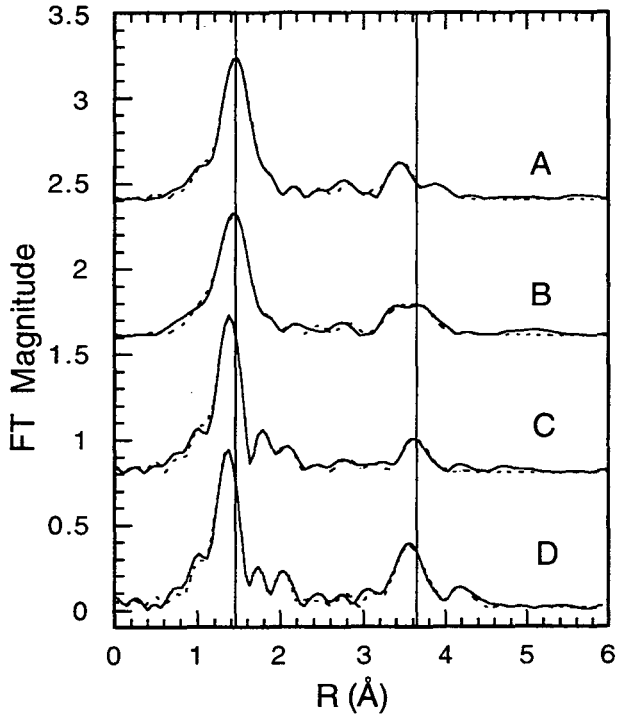

Figure 2

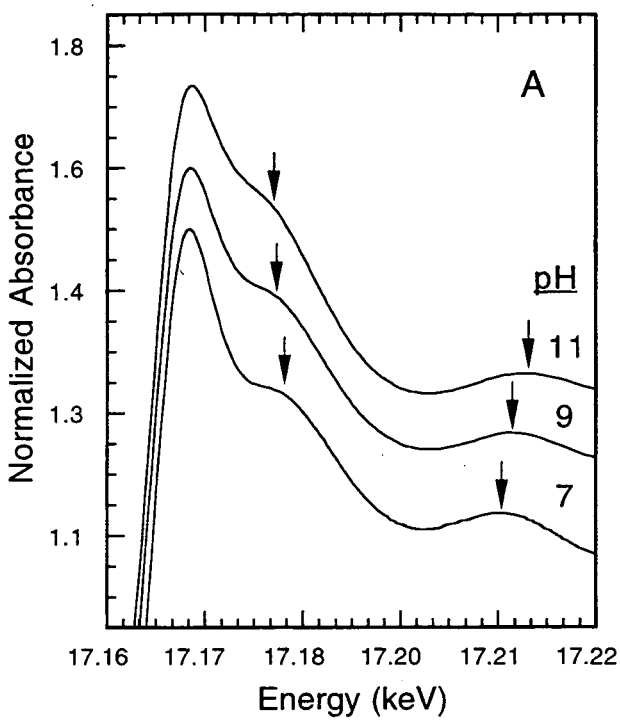
A
pH
11
9
7
Normalized Absorbance
1.8
1.6
1.4
1.3
1.1
17.16
17.17
17.18
17.20
17.21
17.22
Energy (keV)

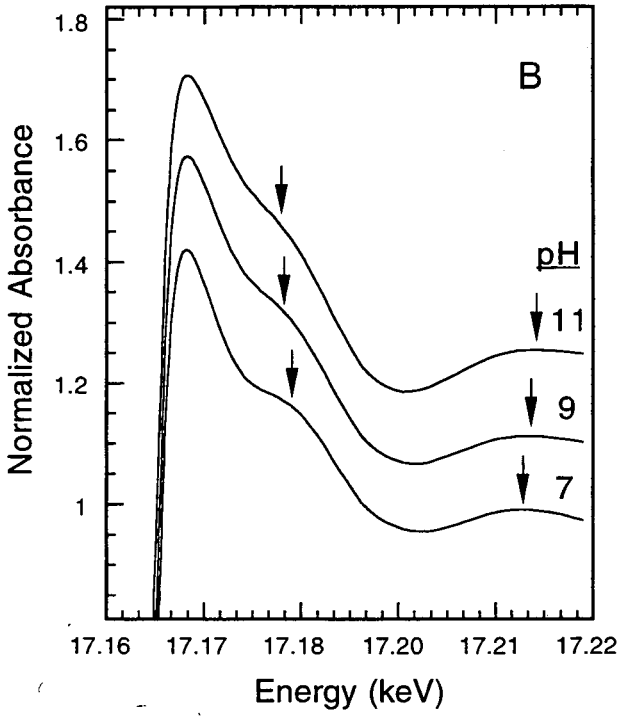
B
pH
11
9
7
Normalized Absorbance
1.8
1.6
1.4
1.2
1
17.16
17.17
17.18
17.20
17.21
17.22
Energy (keV)

Figure 3

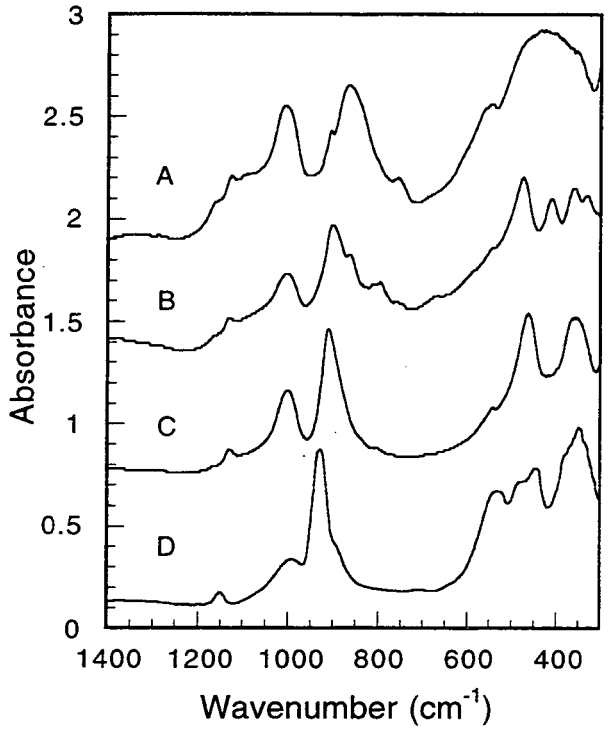
3
2.5
2
1.5
1
0.5
0
Absorbance
A
B
C
D
1400
1200
1000
800
600
400
Wavenumber (cm-1)

Figure 4

A

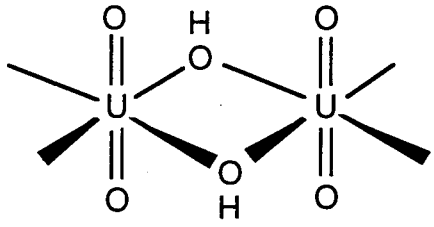

B

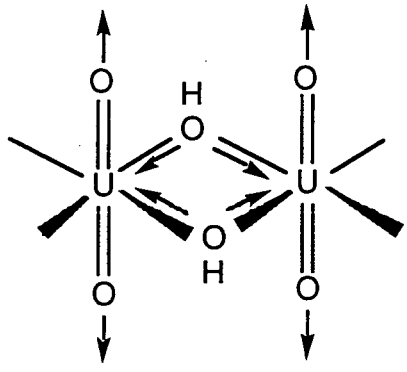

Figure 5

LAWRENCE BERKELEY NATIONAL LABORATORY
UNIVERSITY OF CALIFORNIA
TECHNICAL & ELECTRONIC INFORMATION DEPARTMENT
BERKELEY, CALIFORNIA 94720